Solar-Terrestrial Physics. 2026, vol. 12, iss. 3, pp. 128–136. DOI: 10.12737/stp-123202615. © 2026
I.V. Kichigin, V.P. Tashlykov, V.P. Lebedev, S.S. Alsatkin. *Published by INFRA-M Academic Publishing House*

DOI: 10.12737/stp-123202615
EDN: DBTAWL

Received October 21, 2025
Accepted February 07, 2026

RANGE DETECTION IMPROVEMENT FOR IRKUTSK INCOHERENT SCATTER RADAR MEASUREMENTS WITH BARKER CODE MODULATION

I.V. Kichigin
Irkutsk State University,
Irkutsk, Russia, ivan.kichigin977@iszf.irk.ru
Institute of Solar-Terrestrial Physics SB RAS,
Irkutsk, Russia

V.P. Tashlykov
Institute of Solar-Terrestrial Physics SB RAS,
Irkutsk, Russia, vtashlykov@iszf.irk.ru

V.P. Lebedev
Institute of Solar-Terrestrial Physics SB RAS,
Irkutsk, Russia, lebedev@iszf.irk.ru

S.S. Alsatkin
Institute of Solar-Terrestrial Physics SB RAS,
Irkutsk, Russia, alss@iszf.irk.ru

Abstract. Barker codes are widely used in incoherent scatter (IS) radars, particularly for tasks requiring a significant improvement in spatial resolution. However, sidelobes in the response structure of the correlation processing filter to the probing signal lead to a reduction in the informativeness of ionospheric plasma parameter measurements. This paper investigates the application of a sidelobe-free (SLF) filter for processing signals from the Irkutsk IS radar (IISR). We compare the SLF method with standard matched filtering by analyzing experimental data. The study shows that the SLF filter effectively suppresses sidelobes, which improves the identification of interference from space vehicles and allows for the separation of closely spaced ground clutter sources with improved range resolution. Applying the SLF filter to electron density profile recovery via Faraday rotation demonstrates increased robustness and accuracy, particularly for short integration time (1–2 min). The results confirm that implementing SLF processing for IISR measurements increases the range detection of weak signals and improves spatial resolution from 30 to 6 km by mitigating the masking problem.

Keywords: incoherent scatter radar, range resolution, range detection of informative signals, sidelobe-free decoding filter, spatial resolution, electron density, space objects clutter, ground clutter.

INTRODUCTION

The incoherent scatter (IS) method is the most informative technique for remote ionospheric diagnostics. We can use it to conduct long-term measurements of plasma parameters (electron density, electron and ion temperatures, and ion composition) within the ionosphere at altitudes up to 1000 km. IS radars performing these measurements have stringent requirements for the transmitting and receiving complex, including high peak transmitter power (up to 3.2 MW), high antenna gain, and the ability to generate probing signals with complex modulation types. Such requirements lead to high costs and complexities in developing an IS radar and supporting its operations.

The Irkutsk Incoherent Scatter Radar (IISR) is the only radar of its kind in Russia and one of the few in the world that actively utilizes this method. The IISR operates in the 154–162 MHz frequency range and only with linearly polarized signals [Potekhin et al., 2009]. This setup enables electron density measurements using the Faraday rotation method [Farley, 1969], which imposes strict requirements on range resolution (the minimum distance between distinguishable objects) and the detection performance of weak signals. The latter is limited by the masking of the useful signal by sidelobes from powerful reflections, making it impossible to distinguish weak structures even if they are formally resolved in range. To conduct these measurements, the IISR uses Barker code phase modulation [Barker, 1953].

The goal of this work is to correct the impulse response of the IISR correlation processing filter to achieve full sidelobe suppression and eliminate false detections from interference sources (space vehicles and ground clutter), as well as to increase the accuracy and robustness of ionospheric parameter recovery during short integration times. Note that when operating in dense clutter environments the central task of radar signal design remains the strict control of self-generated sidelobe levels at the filter output, which requires a search for new optimization and coding methods [Singh and Bhatt, 2021]. Our choice in favor of the sidelobe-free (SLF) filter is due to its computational determinism. Unlike adaptive pulse compression (APC) methods or minimum mean square error (MMSE) estimation, which require iterative weight selection for each height window [Blunt and Gerlach, 2006], the SLF filter has a fixed impulse response whose calculation time is negligible compared to the IISR processing cycle.

Despite the high efficiency of modern iterative approaches, such as fast marginal likelihood maximization (FMLM-SBL) [Liu et al., 2022] or the use of generalized Pareto distributions (GPD) to enhance sparsity [Zhang et al., 2022], their application for the IISR is limited by high computational complexity at the system's large degrees of freedom. The SLF filter employed in this work provides the necessary level of sidelobe suppression while maintaining computational determinism, which is critical for real-time IS signal processing.

© 2026 Kichigin I.V. et al.
This article is an open access article distributed under the terms and conditions of the Creative Commons Attribution (CC BY-NC-ND) License (https://creativecommons.org/licenses/by-nc-nd/4.0/).

The SLF filter processing is inevitably accompanied by losses in the main lobe: for the 5-bit Barker code used at the IISR, these losses are ~13.4 % (R=0.866); whereas for a 13-bit code, only 5 % (R=0.952) [Lehtinen et al., 2004]. However, full sidelobe suppression (theoretically down to 10^{-16}) compensates for these losses by eliminating the masking of weak signals and ensuring variance stability, which is critical for the IS method.

The method for calculating the SLF filter impulse response was first proposed in [Rihaczek & Golden, 1971]. A detailed review of such methods can be found in [Blinchikoff and Zverev, 2001]. Regarding the IS method, the use of these filters was studied in detail in [Sulzer, 1989; Damtie et al., 2004] and in [Lehtinen et al., 2004], where the authors proposed a series of optimal binary codes for which the SLF filter has minimal losses in the main lobe of the response structure.

In the last decade, the research in the field of radar has seen a transition toward adaptive methods based on machine learning and Bayesian inference. For example, Generative Adversarial Networks (GANs) have been successfully adopted to suppress active interference, demonstrating superiority over classic Recurrent Neural Network (RNN) methods and time-frequency filtering [Yu et al., 2024]. Parallel to this, Sparse Bayesian Learning (SBL) methods are being developed, which allow for the effective recovery of the interference spectrum with a limited number of training samples [Zhang et al., 2022; Liu et al., 2022].

One of the most important tasks during the planning stage of experimental IS observations is the selection of the probing signal. Its modulation type and envelope shape depend on the object of study. For example, for electron density measurements in the ionospheric F2 layer, the IISR uses a signal phase-modulated with a Barker code with a duration of ~200 μs; for measurements of ionospheric plasma temperatures in the F2 layer, a single amplitude-modulated pulse with a duration of ~700 μs.

The choice of probing signal directly affects the method employed to process the backscattered signal. Correlation signal processing, in which the shape of the filter's impulse response is a mirror image of the transmitted signal waveform, is traditionally known as matched filtering. The primary advantage of Barker-coded signals (compared to simple rectangular pulses) is their spatial selectivity: due to the minimal contribution of the signal response structure sidelobes, it is possible to significantly improve the spatial resolution of measurements. This is particularly important for the IISR when measuring electron density using the Faraday rotation method, where thin structures requiring high resolution may be present. However, although the contribution of the autocorrelation function (ACF) sidelobes is minimal, their presence negatively affects the informativeness of measurements. This becomes most apparent during reflections from several closely spaced objects, such as space vehicles or ground clutter. This drawback is resolved by applying specialized filters that allow for the full suppression of signal sidelobes at the cost of a minor loss in signal power. This method is widely used in traditional radar, where the reliable identification of interference from closely spaced targets is critical.

In describing the matched filtering algorithm, we define the discrete impulse:

$$\delta(n)=\begin{cases}1, \text{ for } n=0\\ 0, \text{ for } n\neq 0\end{cases} \tag{1}$$

and the elementary pulse:

$$p(n)=\sum_{j=0}^{n_s-1}\delta(j-n),\ n=-\infty,...,\infty, \tag{2}$$

where n_s is the number of discrete samples per elementary pulse (bit of the code). Using the δ-function, we can express the response of the coding filter $h_c(n)$, where a_j is an element of the binary sequence, such as a Barker code:

$$h_c(n)=\sum_{j=0}^{n_B-1}a_j\delta(n-jn_s),\ n=-\infty,...,\infty, \tag{3}$$

where n_B is the length of the binary sequence.

Next, we use the concept of convolution. For two numerical sequences $a=\{a_0, a_1, ..., a_{N_1-1}\}$ and $b=\{b_0, b_1, ..., b_{N_2-1}\}$, the length of the resulting output sequence is $N_{out}=N_1+N_2-1$. An element of the new sequence is determined by the following equation:

$$c_i=\sum_{k=0}^{N_1-1}a_k b_{i-k},\ i=0,...,N_{out}-1. \tag{4}$$

We recall the definition of the discrete Fourier transform:

$$X_k=\sum_{n=0}^{N-1}x_n e^{-\frac{2\pi i}{N}kn},\ k=0,...,N-1. \tag{5}$$

The inverse Fourier transform is described by the equation:

$$x_n=\frac{1}{N}\sum_{k=0}^{N-1}X_k e^{\frac{2\pi i}{N}kn},\ n=0,...,N-1. \tag{6}$$

An important property for subsequent calculations is the relationship between the convolution of two sequences and their Fourier transforms:

$$R(f)=F\{u*v\}(f)=U(f)V(f). \tag{7}$$

Based on the definitions above, the result of the convolution of the impulse response of probing signal formation filter (3) and elementary pulse (2):

$$\in(n)=h_c(n)*p(n). \tag{8}$$

To construct a correlation processing filter without sidelobes, we must define its full impulse response λ(*n*), which is the convolution of the impulse response of the decoding filter itself $h_d(n)$ and the filter $q(n)$ designed for processing the elementary pulse $p(n)$. In this work, following the approach of [Lehtinen et al., 2004], we use a matched filter to process the elementary pulse, i.e. $q(n)=p(-n)$; hence

$$\lambda(n)=h_d(n)*q(n). \tag{9}$$

The structure of the filter $h_d(n)$ is determined by a binary weight sequence:

$$h_d(n) = \sum_{j=0}^{n_B-1} b_j \delta(n - jn_s),\ n = -\infty, ..., \infty, \quad (10)$$

where the coefficients b_j are the elements of the original coding sequence a_j taken in reverse order.

By convolving $\lambda(n)$ and $\in(n)$, we obtain a weight function that, in the case of matched filtering, consists of one main lobe and a series of small sidelobes. Nonetheless, if we define $\lambda(n)$ using the formulas below, we can obtain a filter that eliminates the sidelobes:

$$\lambda(n) = \frac{1}{2\pi}\int_{w=0}^{2\pi} \frac{Q(\omega)}{H_c(\omega)} e^{in\omega} d\omega, \quad (11)$$

where

$$Q(\omega) = \sum_{n=-\infty}^{\infty} q(n) e^{-in} \quad (12)$$

and

$$H_c(\omega) = \sum_{n=-\infty}^{\infty} h_c(n) e^{-in\omega}. \quad (13)$$

Applying formulas (11–13) yields the impulse response of the sidelobe-free (SLF) filter. Strictly speaking, such a filter has an infinite impulse response, but its amplitude decays rapidly as the time offset increases, allowing its duration to be limited to a reasonable value. For instance, for the standard IISR signal with a 200 μs duration modulated by a 5-bit Barker code with 4 μs discrete samples, this duration is 600 μs. Figure 1 shows the forms of the impulse response for both the matched filter (MF) and the SLF filter. Importantly, the SLF filter impulse response can be calculated only if there are no zeros in the spectrum of the function $h_c(n)$, which is true for most binary sequences, including Barker codes.

When processing with the SLF filter, it is necessary to account for the height shift h' that occurs during signal convolution with the filter response. The observed shift of the main peak of the filtered signal can be determined by the formula:

$$h' = (h + T/2 + n), \quad (14)$$

where h' is the corrected height, h is the uncorrected height, T is the number of samples in the filter's impulse response, and n is the number of samples in one bit of the code.

To assess the effectiveness of the SLF filter for practical IISR measurements, we examine the three most common sources of reflected and/or scattered signals: space vehicles, ground clutter, and the ionosphere.

1. INTERFERENCE FROM SPACE VEHICLES

Reflections from artificial space vehicles (SVs) in IISR data appear as short sharp pulses at specific altitudes, which introduce interference into ionospheric measurements. Such peaks complicate the analysis of weak ionospheric signals and are frequently tracked for space monitoring purposes; however, they must be excluded for atmospheric studies.

Some SV passes are observed outside the main lobe of the antenna beam through sidelobes, where the reception level is significantly lower, resulting in a very weak radio signal [Lebedev, 2015]. Under these conditions, the classic filtering method produces a very low signal-to-noise ratio (SNR) and numerous false responses. The application of the sidelobe-free (SLF) filter simplifies the selection of weak signals and the identification of false responses occurring during reception through antenna sidelobes. IISR experimental data confirms that the SLF filter simplifies the detection and suppression of interference from passing satellites. Essentially, the elimination of range sidelobes makes it possible to automatically isolate the satellite echo and exclude it from further analysis of ionospheric profiles.

Figure 2 gives two examples of a signal containing satellite interference with low Doppler velocity (within the main antenna lobe). The red curve represents the matched filtering result; the blue curve, the SLF processing result. Comparison of filtering efficiency for different satellite pass scenarios has revealed the following:

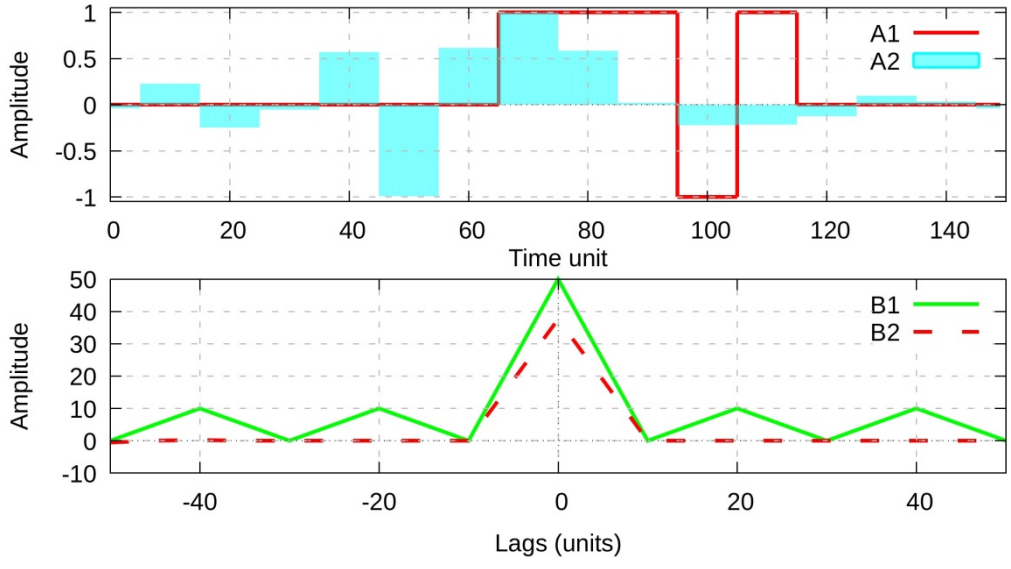

Figure 1. Comparison between results from matched filtering and SLF (sidelobe-free) processing: A1 — MF impulse response; A2 — SLF filter impulse response (shifted by the delay value determined by Eq. 14); B1 — ACF during matched filtering; B2 — ACF during SLF filtering

- Reception via the main antenna lobe (strong signal): The primary advantage of the SLF filter is the increased accuracy of range determination by narrowing the response and eliminating ACF “tails” that could be misinterpreted as secondary targets (space debris).
- Reception via antenna sidelobes (weak signal): The SLF filter plays a decisive role in ensuring detectability. Eliminating the sidelobes of the response structure reduces the detection threshold by excluding the amplitude masking (masking problem) of the weak signal by its own range sidelobes, whose level in matched filtering is comparable to the noise level.

Note that the effectiveness of sidelobe suppression by the SLF filter decreases in the presence of a significant Doppler shift. This issue can, however, be addressed during the iterative calculation of SV coordinate characteristics by introducing a Doppler velocity hypothesis prior to correlation processing. Further development of this approach, including the software implementation of the SLF filter for determining space vehicle coordinates and performing statistical analysis of the obtained data, is currently the subject of ongoing research for a future publication. By incorporating the known Doppler velocity of a vehicle, the SLF filter can be employed to eliminate sidelobes in a more precise manner, which is critical for improving the accuracy of SV localization and effectively isolating the range intervals where ionospheric measurements are contaminated by satellite echoes. Such an approach will provide more reliable selection of the useful signal in a complex interference environment.

2. GROUND CLUTTER IDENTIFICATION

One of the significant problems for the IISR, common to most incoherent scatter (IS) radars, is the constant presence of interference in the 100–300 km range interval, arising from reflections of antenna beam sidelobes by ground objects (primarily the Eastern Sayan mountains). This significantly complicates the analysis of D- and E-layer ionospheric parameters. In [Turunen et al., 2000; Lehtinen et al., 2002], methods for subtracting such interference are proposed which open the possibility of analyzing the useful signal at these ranges. Due to the stationary nature of terrain features and their large scattering cross-sections, ground clutter echoes are much stronger than the IS signal, allowing for reliable detection, yet weak echoes related to refraction are often observed, which can introduce significant errors. The application of the SLF filter shows that these interferences are detected more reliably than with matched filtering (Figures 3, 4, 5). Moreover, SLF processing identifies objects that remain indistinguishable under matched filtering due to resolution limitations (30 km vs. 6 km for the SLF filter).

It must be clarified that although the theoretical range resolution for both methods is determined by the duration of the elementary pulse (40 μs) and equals ~6 km, the practical selectivity of the matched filter (MF) is limited by its impulse response. The MF generates a “"pedestal” of sidelobes distributed across the entire duration of the probing signal (200 μs, 30 km).

In the case of a solitary target with a high SNR, both filters can separate objects at a distance of 6 km. However, when multiple targets are present or the SNR decreases, the MF sidelobes create a masking problem, where weak signals “sink” into the energy trail of more powerful neighboring reflections. Thus, the MF realizes a 6 km resolution only under ideal conditions; in real interference environments, its resolution may degrade to the duration of the entire pulse (200 μs, 30 km). Implementing SLF processing allows for the stabilization of range resolution at the 6 km level regardless of dynamic range or target proximity by unmasking weak structures.

We examined the signal reflected from the terrain during IISR measurements on September 19, 2023 (frequency 159.5 MHz, 1-minute integration). The transmitted signal was phase-modulated with a 5-bit Barker code (200 μs total duration; 40 μs bit duration). Figure 3 illustrates the SNR for the 100–140 km altitude range.

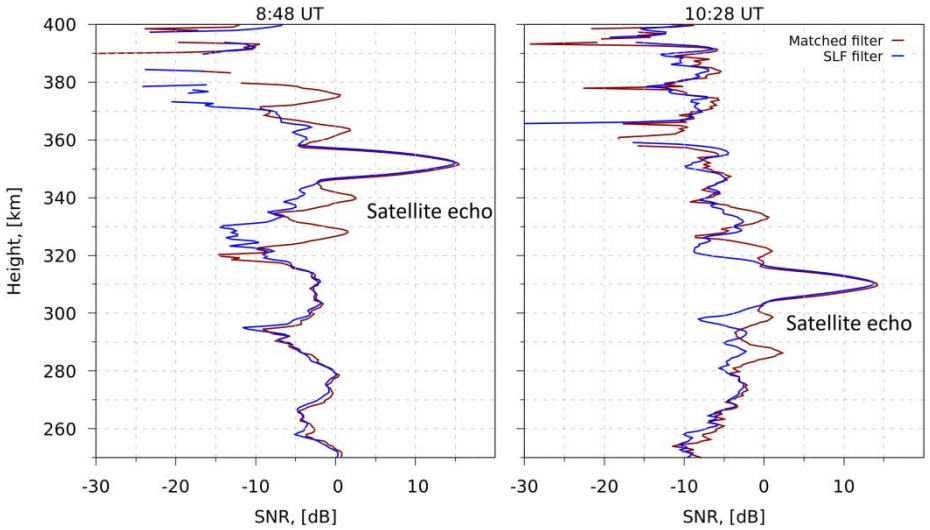

Figure 2. Examples of detectable interference from space vehicles (SVs) for IISR measurements on December 3, 2023 (155 MHz frequency, 1-min integration)

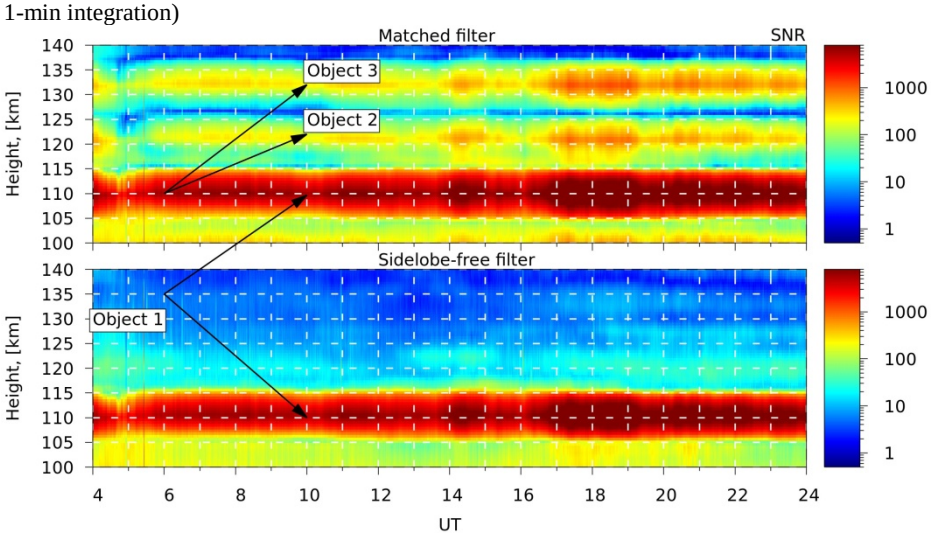

Figure 3. SNR according to IISR measurement data on September 19, 2023 (altitude range 100–140 km). Top panel — MF processing, bottom panel — SLF processing

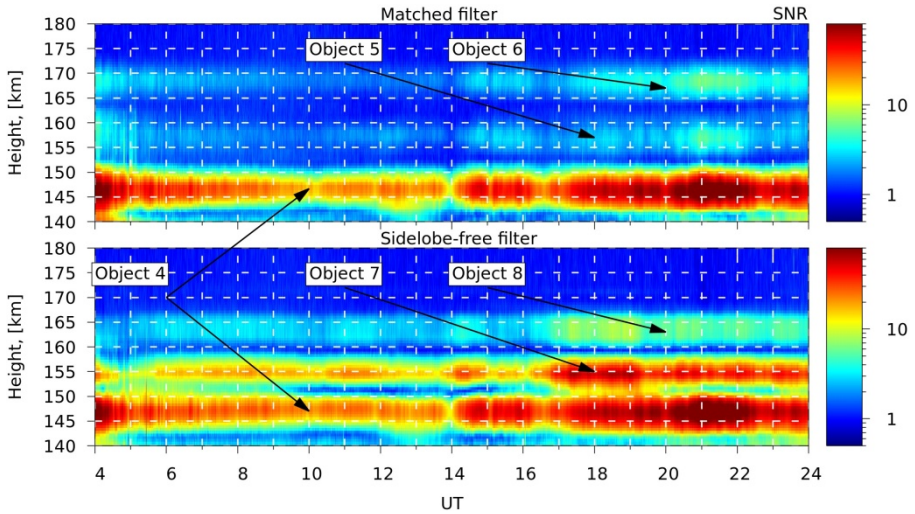

Figure 4. The same as in Figure 3 for the altitude range 140–180 km

Object 1 (Figure 3) corresponds to the main peak of the MF correlation response and indicates an echo from a mountain peak located ~110 km from the IISR. We assume that temporal power variations are caused by

© 2026 Kichigin I.V. et al.
This article is an open access article distributed under the terms and conditions of the Creative Commons Attribution (CC BY-NC-ND) License (https://creativecommons.org/licenses/by-nc-nd/4.0/).

radio signal refraction and reflect the dynamics of tropospheric parameters (temperature, pressure, humidity). Objects 2 and 3 exhibit temporal power dynamics identical to Object 1, leading to the conclusion that they represent the sidelobes of the MF correlation response. Because the mountain peak is stationary, these sidelobes are absent in SLF processing (Figure 3, bottom panel); however, new echoes appear, likely due to signal refraction resulting from shifting cloud cover or precipitation.

Figure 4 displays the SNR for the 140–180 km range. Using similar reasoning as for Objects 1–3 (Figure 3), we can show that Objects 4–6 represent the main peak and sidelobes respectively (peak range ~147 km). Despite their similarity to Objects 5 and 6, Objects 7 and 8 are most likely independent reflections received through a different antenna sidelobe at a different angle of arrival. As shown through modeling, matched filtering loses the ability to reliably detect multiple objects if they are closer than 30 km to one another; SLF processing separates objects at 6 km. Thus, Objects 7 and 8 are reflections from terrain features at ranges of ~155 and ~161 km respectively. They are not detected during matched filtering due to the amplitude masking ([Blunt, Gerlach, 2006]) of their weak reflections by powerful neighboring Object 4.

Statistical analysis confirms the independence of these objects. For the MF, the Pearson correlation coefficient between power at ~147 and ~167 km was ~0.7, indicating a strong dependence due to sidelobes. With SLF processing, the correlation drops to ~0.28, proving that the radar captures independent reflections from different terrain elements. Figure 5 shows the SNR for the 160–200 km range, where the IS signal begins to be detected. SLF processing reveals a new interference at ~190 km, likely from Starlink simulators or interference from different ranges/angles.

2. ELECTRON DENSITY MEASUREMENTS VIA FARADAY ROTATION

The IISR can directly record Faraday rotation — phase shifts between orthogonal polarizations — to reconstruct vertical electron density N_e profiles in the F

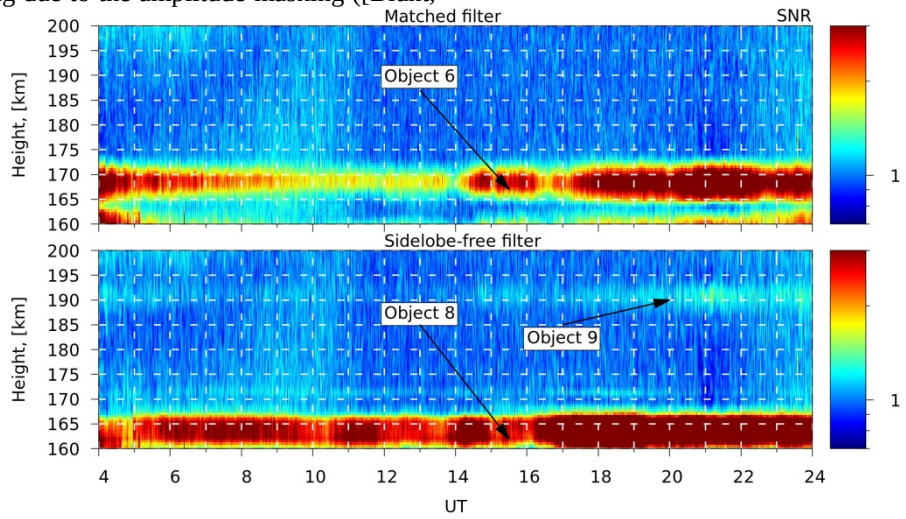

Figure 5. The same as in Figure 3 for the altitude range 160–200 km

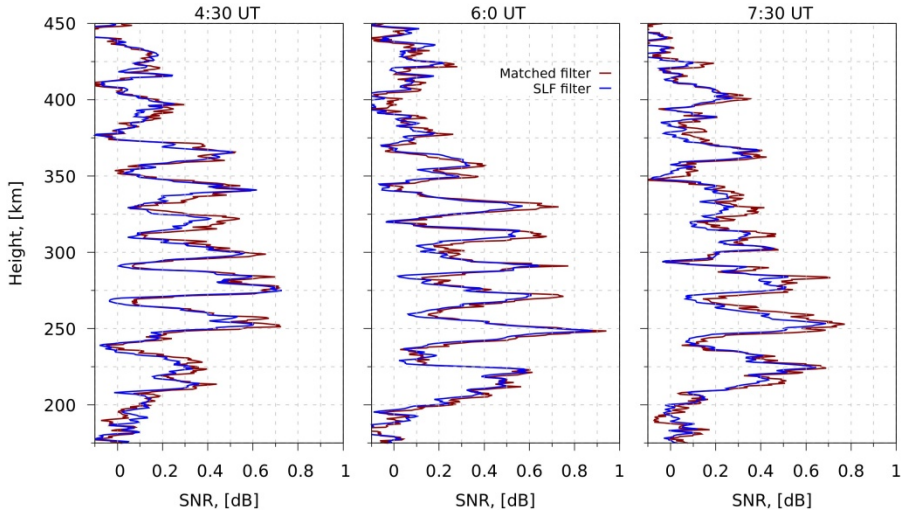

Figure 6. Comparison between SNR profiles for matched filtering and SLF filtering. Accumulation was performed over a 2-min interval (200 realizations)

layer. This procedure is based on solving an inverse problem and is highly sensitive to interference.

Experimentally, the advantage of SLF processing in N_e profile reconstruction is most evident with a limited number of pulse accumulations. If minor averaging is conducted (e.g., dozens of realizations), sidelobes from weak structures are noticeable, and SLF processing demonstrates a clear increase in profile accuracy (Figure 6). At high accumulations (~1000), the difference practically disappears.

Figure 6 compares the power profiles of matched and SLF (sidelobe-free) processing for 04:30, 06:00, and 07:30 UT on September 19, 2023 (159.5 MHz frequency, 1-min integration). The depth of Faraday fading with SLF processing is significantly lower than with matched filtering. This enables better resolution of measurement uncertainty in height, particularly when the length of the modulating sequence is poorly chosen (for measurements with a high expected SNR, a 13-bit Barker code is generally applied at the IISR).

Analysis of the Faraday fading profile allows for the recovery of absolute values of the N_e profile [Alsatkin et al., 2020]. However, as noted above, analysis of the power profile during SLF processing is most justified with small accumulations of signal realizations (integration time ≤2 min). The current procedure for statistical analysis and N_e profile fitting for the IISR, based on a brute-force search of the desired parameters, is not adapted for the operational analysis of data with such temporal resolution. To solve this problem, we applied a nonlinear regression (fitting) algorithm for the N_e profile based on an evolutionary strategy, which was previously used successfully for IISR data [Tashlykov et al., 2024]. This algorithm requires significantly fewer iterations to find a global optimum and is more easily parallelized for computations.

The experimental power and the model power, obtained through the nonlinear regression of N_e, are compared in Figure 7. It should be noted that one of the main disadvantages of the approach based on fitting the full N_e profile remains the lack of robustness, where the presence of even weak interference can significantly distort the resulting N_e profile. Therefore, in the analysis of IISR data, a lower height boundary is usually established

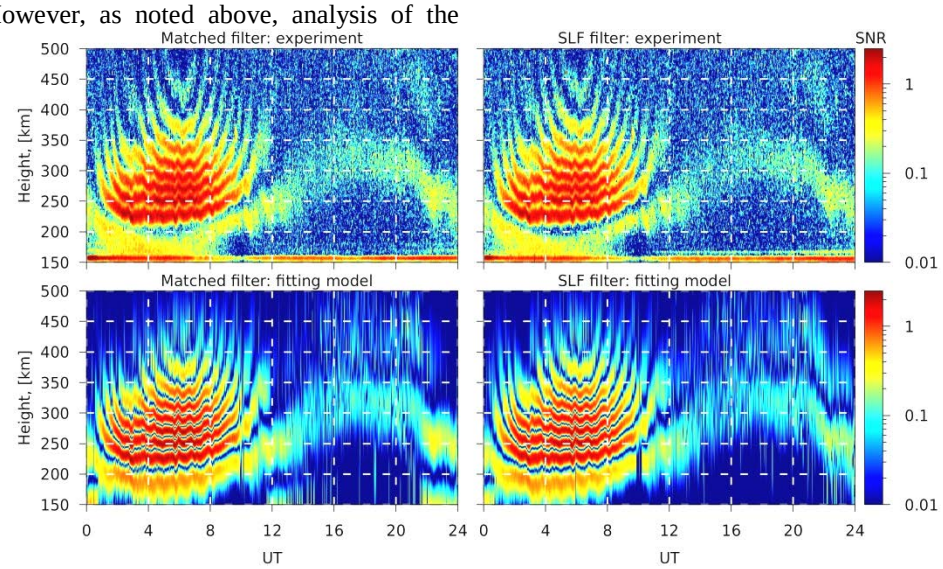

Figure 7. Comparison between SNR for IISR measurements (December 3, 2023, 155 MHz frequency, 1-min integration). Top left panel — matched filter processing result. Top right panel — SLF processing result. Bottom left panel — model SNR obtained through nonlinear regression of the electron density (N_e) profile for matched filtering. Bottom right panel — model SNR from nonlinear regression of the electron density (N_e) profile for SLF processing

empirically, from which a correct analysis can begin. In this case, we deliberately lowered this lower boundary (down to 160 km), capturing weak ground clutter interference (up to 170 km), to demonstrate another non-obvious advantage of SLF (sidelobe-free) processing. During matched filtering, interference at 160–170 km altitudes is interpreted by the model as an additional maximum (around 12 and 23 UT, left panels in Figure 7), which significantly distorts the final N_e profile. With SLF processing (see right panels in Figure 7), such artifacts are absent, as the more pronounced and narrow shape of the interference prevents the model from fitting an additional power maximum better than its absence would allow.

To quantitatively assess the approximation accuracy, the Mean Square Error (MSE) of the model power profiles relative to the experimental data was calculated for the moments in time shown in Figure 6. The use of mean square error as an indicator of convergence stability and approximation quality is an accepted standard in modern adaptive filtering systems and allows for the quantitative evaluation of the degree of waveform distortion caused by sidelobes [Shen et al., 2024]. For matched filtering, the MSE values were 0.093, 0.08, and 0.054 (for 04:30, 05:00, and 06:30 UT respectively). When using the SLF filter, the error decreased to 0.039, 0.066, and 0.042 respectively. This reduction in MSE is due to the fact that the SLF filter more effectively sup-

© 2026 Kichigin I.V. et al.
This article is an open access article distributed under the terms and conditions of the Creative Commons Attribution (CC BY-NC-ND) License (https://creativecommons.org/licenses/by-nc-nd/4.0/).

presses power in the minima of Faraday fading, eliminating the "illumination" of these zones by the sidelobes of neighboring maxima (the masking problem). This allows the experimental profile to correspond more deeply to the theoretical model, which is critical for the reliable estimation of ionospheric parameters at short integration times (1–2 min).

In IISR measurement practice, the manifestation of ground clutter is often observed at altitudes above the empirically set boundary of 170 km, especially at night when a sharp drop in temperature significantly enhances signal refraction. The application of the new N_e profile recovery algorithm will help partially solve this problem. The task of automatic and reliable identification of ground clutter requires further consideration. Another important advantage of the algorithm we use is its speed, which allows for the operational analysis of IISR data with high temporal resolution. This is relevant for analyzing the traces of ionospheric irregularities in the IISR signal. For example, in Figure 7 (top panels) in the 6–8 UT interval, we can see clear traces of traveling ionospheric disturbances (TIDs), which demonstrate much less obvious signs with longer integration times.

3. RECOMMENDATIONS FOR THE PRACTICAL USE OF SLF FILTERING

Based on the research conducted, five priority scenarios for the application of SLF processing in the standard IISR data processing cycle can be identified.

1. *Measurements at high N_e*

During periods of high solar activity, when the N_e profile is characterized by a large number of Faraday rotations, the use of the SLF filter provides a gain comparable to switching to longer codes (e.g., from 5-bit to 13-bit Barker code). Since the SLF filter is a post-processing method, it allows the data quality to be improved without changing the hardware settings of the transmitter.

2. *Improving the accuracy of space vehicle trajectory measurements*

The elimination of ACF tails will allow for more accurate determination of the coordinate characteristics of space vehicles (SVs) and the identification of small-sized space debris. This direction is promising for future research on monitoring near-Earth space.

3. *Controlling group interference from satellite constellations*

One of the current problems is the contamination of the signal by "swarms" of low-orbit satellites (such as Starlink). Due to their small scattering cross-section and large numbers, the interfering signals are extremely difficult to separate from the ionospheric response. The improved range detectability of the SLF filter may allow for the effective unmasking of the useful signal under such conditions.

4. *Analysis of the lower ionosphere layers D and E*

After subtracting ground clutter, which has been cleared using the SLF filter, the possibility opens up for systematic analysis of D- and E-layer parameters. This was previously not conducted at the IISR due to the strong masking influence of the Eastern Sayan mountains. The ground clutter subtraction method is currently under development.

5. *Diagnostics of tropospheric parameters*

Monitoring the temporal dynamics of the identified stable ground echoes (see Figure 4) allows for the recovery of the radio wave refraction coefficient, which provides indirect information on the dynamics of temperature and humidity in the lower layers of the atmosphere.

CONCLUSION

We have carried out a comprehensive study on the application of a sidelobe-free (SLF) correlation processing filter to enhance the quality of IISR measurements. The primary focus was on solving practical problems associated with interfering reflections from space vehicles and ground clutter, as well as on improving the accuracy of electron density (N_e) profile reconstruction via Faraday rotation.

The SLF filter demonstrated high effectiveness in suppressing the sidelobes of the correlation response structure. This filter characteristic significantly improved the detection of signals from SVs with low Doppler velocity, increasing the main lobe power to background noise ratio and reducing the number of "noisy" altitude samples of the signal. The elimination of sidelobes simplifies the automation of detection and exclusion procedures for such interference from the data. Implementing SLF processing resulted in a fivefold increase in the spatial resolution of the IISR from 30 to 6 km for a 200-μs pulse (5-bit Barker code). This allows us to unmask potential ionospheric structures previously hidden beneath the sidelobes of powerful reflections from the Eastern Sayan mountains (suppression level more than 20 dB relative to standard filtering).

When analyzing ground clutter, we confirmed that the SLF filter provides significantly higher range resolution compared to standard matched filtering. For the most frequently used IISR signal (5-bit Barker code modulating a 200-μs pulse), SLF processing allows for the separation of closely spaced interference sources (mountain peaks) at a distance of ~6 km, whereas for a matched filter this limit is ~30 km. This opens up the possibility for more detailed mapping of interfering reflection sources and for studying refraction effects in the troposphere.

Comparative analysis shows that while deep learning methods (GAN) [Yu et al., 2024] are oriented toward noisy signal recovery under active counteraction, and SBL methods are aimed at optimizing performance in non-uniform interference [Zhang et al., 2022; Liu et al., 2022], the SLF filter solves the specific problems of eliminating the masking influence of sidelobes from powerful terrain reflections, providing a fivefold increase in spatial resolution.

During reconstruction of the N_e profile via Faraday rotation, the main advantage of SLF processing is evident at short integration times (~1–2 min). Under these conditions, the filter provides a clearer and smoother

power profile with a reduced fading depth, which decreases measurement uncertainty. Furthermore, we have shown that using the SLF filter in combination with an evolutionary algorithm for reconstructing the N_e profile prevents the appearance of artifacts in the form of false concentration maxima caused by weak ground clutter, thereby increasing the robustness of the method.

Thus, the practical implementation of SLF filtering in IISR data processing is a highly effective method for increasing the informativeness of measurements. The proposed approach can simultaneously solve several pressing problems: improving the identification and filtering of interfering reflections, increasing range resolution and the accuracy of determining key ionospheric plasma parameters in modes critical to interference levels and integration times. The improvement in the range detectability of informative reflections potentially opens up the possibility for measurements of the sporadic-E (E_s) layer [Turunen et al., 1985; Damtie et al., 2002], which have not previously been conducted at the IISR. Future research will be directed toward adapting the method to signals from SVs with high Doppler frequencies and toward the development of fully automated algorithms for interference identification.

The work was financially supported by the Ministry of Science and Higher Education of the Russian Federation. The work used measurement data from the Large-Scale Research Facility “Irkutsk Incoherent Scatter Radar” of ISTP SB RAS [http://ckp-rf.ru/usu/77733/].

REFERENCES

Alsatkin S.S., Medvedev A.V., Ratovsky K.G. Features of N_e recovery at the Irkutsk Incoherent Scatter Radar. *Sol.-Terr. Phys*. 2020, vol. 6, iss. 1, pp. 77–88. https://doi.org/10.12737/stp-61202009.

Barker R.H. Group synchronizing of binary digital systems. *Communication Theory*. London: Butterworth, 1953, pp. 273–287.

Blinchikoff H.J., Zverev A.I. *Filtering in the Time and Frequency Domains*. Raleigh, NC: SciTech Publishing, Inc., 2001, 487 p.

Blunt S.D., Gerlach K. Adaptive pulse compression via MMSE. *IEEE Transactions on Aerospace and Electronic Systems*. 2006, vol. 42, iss. 2, pp. 572–584. https://doi.org/10.1109/TAES.2006.1642573.

Damtie B., Nygrén T., Lehtinen M.S., et al. High resolution observations of sporadic-E layers within the polar cap ionosphere using a new incoherent scatter radar experiment. *Ann. Geophys.* 2002, vol. 20, iss. 9, pp. 1429–1438. https://doi.org/10.5194/angeo-20-1429-2002.

Damtie B., Lehtinen M.S., Nygrén T. Decoding of Barker-coded incoherent scatter measurements by means of mathematical inversion. *Ann. Geophys.* 2004, vol. 22, iss. 1, pp. 3–13. https://doi.org/10.5194/angeo-22-3-2004.

Farley D.T. Faraday rotation measurements using incoherent scatter. *Radio Sci*. 1969, vol. 4, iss. 2, pp. 143–152. https://doi.org/10.1029/RS004i002p00143.

Lebedev V.P. [Development of diagnostic capabilities of the Irkutsk Incoherent Scatter Radar for solving problems of spacecraft control and conducting active space experiments]. Cand. tech. sci. diss. Irkutsk, 2015, 145 p. (In Russian).

Lehtinen M.S., Markkanen J., Väänänen A., et al. A new incoherent scatter technique in the EISCAT Svalbard Radar. *Radio Sci*. 2002, vol. 37, iss. 4, pp. 3-1–3-14. https://doi.org/10.1029/2001RS002518.

Lehtinen M.S., Damtie B., Nygrén T. Optimal binary phase codes and sidelobe-free decoding filters with application to incoherent scatter radar. *Ann. Geophys*. 2004, vol. 22, iss. 4, pp. 1623–1632. https://doi.org/10.5194/angeo-22-1623-2004.

Liu C., Wang T., Zhang S., et al. A fast space-time adaptive processing algorithm based on sparse Bayesian learning for airborne radar. *Sensors*. 2022, vol. 22, iss. 7, article 2664. https://doi.org/10.3390/s22072664.

Potekhin A.P., Lebedev V.P., Kurkin V.I., et al. Recording and control digital systems of the Irkutsk Incoherent Scatter Radar. *Geomagnetism and Aeronomy*. 2009, vol. 49, iss. 7, pp. 1011–1021. https://doi.org/10.1134/S0016793209070299.

Rihaczek A.W., Golden R.M. Range sidelobe suppression for Barker codes. *IEEE Transactions on Aerospace and Electronic Systems*. 1971, vol. AES-7, iss. 6, pp. 1087–1092. https://doi.org/10.1109/TAES.1971.310135.

Shen W., Chen X., Zhang Y., et al. A concise and adaptive sidelobe suppression algorithm based on LMS filter for pulse-compressed signal of Φ-OTDR. *Photonics*. 2024, vol. 11, iss. 1, article 70. https://doi.org/10.3390/photonics11010070.

Singh S.P., Bhatt T.D. Sidelobes reduction technique for biphase Barker codes. *International J. Engineering Trends and Technology*. 2021, vol. 69, iss. 6, pp. 239–242. https://doi.org/10.14445/22315381/IJETT-V69I6P234.

Sulzer M.P. Recent incoherent scatter techniques. *Adv. Space Res*. 1989, vol. 9, iss. 5, pp. 153–162. https://doi.org/10.1016/0273-1177(89)90353-0.

Tashlykov V.P., Alsatkin S.S., Medvedev A.V., Ratovsky K.G. Effective subtraction technique: implementation for Irkutsk Incoherent Scatter Radar. *Sol.-Terr. Phys*. 2024, vol. 10, iss. 1, pp. 63–67. https://doi.org/10.12737/stp-101202409.

Turunen T., Silén J., Nygrén T.et al. Observation of a thin E_s layer by the EISCAT radar. *Planetary and Space Science*. 1985, vol. 33, iss. 12, pp. 1509–1514. https://doi.org/10.1016/0032-0633(85)90116-3.

Turunen T., Markkanen J., van Eyken A.P. Ground clutter cancellation in incoherent radars: solutions for EISCAT Svalbard radar. 2000. *Proc. the Tenth EISCAT Workshop*. URL; https://hal.archives-ouvertes.fr/hal-00316795 (accessed June 1, 2024).

Yu Y., You Y., Wang P., et al. Radar active oppressive interference suppression based on generative adversarial network. *IET Radar, Sonar & Navigation*. 2024, vol. 18, iss. 7, pp. 1193–1202. https://doi.org/10.1049/rsn2.12556.

Zhang S., Wang T., Liu C., et al. A space-time adaptive processing method based on Sparse Bayesian Learning for Maneuvering Airborne Radar. *Sensors*. 2022, vol. 22, iss. 15, article 5479. https://doi.org/10.3390/s22155479.

URL: http://ckp-rf.ru/usu/77733/ (accessed April 27, 2026).

Original Russian version: Kichigin I.V., Tashlykov V.P., Lebedev V.P., Alsatkin S.S., published in Solnechno-zemnaya fizika. 2026, vol. 12, no. 3, pp. 142–152. https://doi.org/10.12737/szf-123202615. © 2026 INFRA-M Academic Publishing House (Nauchno-Izdatelskii Tsentr INFRA-M).

How to cite this article

Kichigin I.V., Tashlykov V.P., Lebedev V.P., Alsatkin S.S. Range detection improvement for Irkutsk Incoherent Scatter Radar measurements with Barker code modulation. *Sol.-Terr. Phys*. 2026, vol. 12, iss. 3, pp. 128–136. https://doi.org/10.12737/stp-123202615.